Distributed Secondary Frequency Control in Microgrids: Robustness and Steady-State Performance in the Presence of Clock Drifts ☆

Ajay Krishna[a], Johannes Schiffer[b], Jörg Raisch[a,c]

[a] *Fachgebiet Regelungssysteme, Technische Universität Berlin, Germany.*
[b] *Fachgebiet Regelungssysteme und Netzleittechnik, Brandenburgische Technische Universität Cottbus-Senftenberg, Germany.*
[c] *Max-Planck-Institut für Dynamik komplexer technischer Systeme, Magdeburg, Germany.*

Abstract

Microgrids are distributed systems with high share of inverter-interfaced renewable energy sources where stable and reliable system operation is realized by suitably controlling the inverters. In this work, we focus on secondary frequency control, which is an important ancillary service provided by the inverters. In the literature on secondary frequency control, the effect of *clock drifts* has often been neglected. However, clock drifts are practically unavoidable parameter uncertainties in inverter-based microgrids and we show that the most commonly employed distributed secondary frequency controllers exhibit performance deteriorations when taking clock drifts explicitly into consideration. Motivated by this, we propose a novel alternative control law called *generalized distributed averaging integral* (GDAI) control, which achieves the secondary control objectives of steady-state accurate frequency restoration and proportional power sharing in the presence of clock drifts. In addition, we derive a sufficient tuning criterion in the form of a set of linear matrix inequalities (LMIs) which guarantees robust stability of the closed-loop equilibrium point in the presence of uncertain clock drifts. Finally, our analysis is validated extensively via simulation with comprehensive comparisons to other related distributed control approaches.

1. Introduction

1.1. Motivation and related work

Electric power systems are on the verge of a major structural and technological transformation; structural, because power generation is moving from a fairly small number of large central power stations to a large number of distributed generation units; technological, because in contrast to conventional power networks, the new or so-called *smart grid* (Farhangi, 2010) has the major share of power generation coming from inverter-interfaced renewable energy sources (RESs). The physical characteristics of inverters largely differ from those of conventional generators. Therefore, novel control strategies are needed to ensure stable and reliable power system operation. In this context, the concept of microgrids (MGs) is foreseen as a promising solution (Lasseter, 2002; Hatziargyriou et al., 2007). A MG is a locally controllable subset of a large power system. It consists of several RESs, storage units and corresponding loads. A MG can typically work in islanded or grid-tied mode (Lasseter, 2002; Hatziargyriou et al., 2007). In islanded mode, the units within the MG are responsible for addressing control tasks such as frequency stability, voltage stability and desired power sharing at steady-state, see e.g., (Schiffer, 2015). With high share of RESs, maintaining frequency stability in islanded MGs where both load and generation evolutions are uncertain, is a challenging control task. Therefore, in this paper, we focus on frequency control in islanded MGs.

In conventional power systems, synchronous generators which operate as grid forming units are employed to accomplish this control objective. In inverter-based MGs, inverter-interfaced sources or, more precisely, grid forming inverters (GFIs) have to replace synchronous generators (Lopes et al., 2006). A GFI is a voltage source inverter controlled using voltage and frequency references (Lopes et al., 2006; Schiffer et al., 2017b).

Inspired by conventional power systems, a hierarchical control strategy is often advocated to control an is-

☆ The project leading to this manuscript has received funding from the German Academic Exchange Service (DAAD) and the European Union's Horizon 2020 research and innovation programme under the Marie Skłodowska-Curie grant agreement No. 734832.

Email addresses: krishna@control.tu-berlin.de (Ajay Krishna), schiffer@b-tu.de (Johannes Schiffer), raisch@control.tu-berlin.de (Jörg Raisch)

landed MG, see e.g., (Guerrero et al., 2013; Hans et al., 2014). This hierarchical control structure has primary, secondary and energy management layers. The primary control layer consists of a decentralized proportional control, called *droop control*, which is responsible for maintaining frequency stability along with proportional power sharing (Chandorkar et al., 1993). Despite many advantages, a major drawback of the primary droop control law is that the steady-state frequency usually deviates from its nominal value (50 or 60 Hz). However, since many devices are designed to operate at the nominal frequency value, correcting this frequency deviation is important. Conventionally, a central integral secondary control law (Guerrero et al., 2013) is advocated for this task, where a central unit communicates with all the GFIs. Yet, considering the increasing complexity and the huge number of generation units connected in a MG, centralized approaches significantly increase the communication burden and are also vulnerable to single-point-failures. As a consequence, distributed secondary control architectures are being increasingly proposed for this task (Bidram et al., 2014; Simpson-Porco et al., 2015; Zhao et al., 2015; Schiffer et al., 2017a; Fu et al., 2016; Persis et al., 2016).

Typically, distributed secondary frequency control is implemented by means of *consensus-based* algorithms where the agents in the network reach an agreement by communicating with their neighbors, see e.g., (Olfati-Saber et al., 2007). Since such distributed approaches obviate the requirement for a central communication unit, the overall communication burden in the network is reduced and the reliability is improved (Bidram et al., 2014). Therefore, in this paper, we focus on *distributed secondary frequency control* in inverter-based islanded MGs.

An inverter-based MG involves distributed computation, which is carried out on the digital-controller of each GFI. It is a well known fact that the clocks used to generate time signals of these digital-controllers are not synchronized (Kopetz, 2011; Anritsu, 2001). This results in *clock drifts* between the inverters. In MGs, clock drifts create frequency mismatches (Schiffer et al., 2017b). In the context of distributed secondary frequency control, approaches presented in the literature often neglect the effect of clock drifts. For example, see (Bidram et al., 2014; Simpson-Porco et al., 2015; Zhao et al., 2015; Schiffer et al., 2017a; Fu et al., 2016; Persis et al., 2016). However, recently it has been highlighted that clock drifts have an adverse effect on the performance of secondary frequency control (Castilla et al., 2017, 2018; Martínez et al., 2017; Rosero et al., 2017b; Martí et al., 2018). For example, in (Rosero et al., 2017a), the detrimental effect of clock drifts on the distributed averaging integral (DAI) controller is investigated and it is shown that the DAI controller is unable to properly achieve usual secondary frequency control objectives in the presence of clock drifts. Moreover, in (Martí et al., 2018), a comparative study comprising droop-only, droop-free and various consensus-based distributed approaches in the presence of clock drifts is presented. The authors conclude that all the approaches studied in (Martí et al., 2018) exhibit problems in achieving secondary frequency control objectives in the presence of clock drifts.

In (Castilla et al., 2017), steady-state and transient performance of various decentralized secondary frequency controllers in the presence of clock drifts are compared. In a similar spirit, in (Castilla et al., 2018), a decentralized secondary control approach is studied and the robustness of this approach towards clock drifts under high load conditions is evaluated experimentally. Although decentralized secondary controllers avoid the burden of communication, they have the disadvantage that they exhibit inefficient allocation of generation resources and suffer from poor robustness to measurement bias (Weitenberg et al., 2018). In (Martínez et al., 2017), a droop-free controller which requires neighboring node communication is studied in the presence of clock drifts. However, in the comparative study presented in (Martí et al., 2018), it is shown that the aforementioned droop-free approach does not achieve steady-state power sharing in the presence of clock drifts.

In (Rosero et al., 2017b), a consensus-based distributed frequency controller is studied and the authors confirm experimentally that clock drifts induce power sharing errors and frequency deviations. However, the approach investigated in (Rosero et al., 2017b) requires that each unit communicates with all other units in the MG. In practice, such an all-to-all communication is undesirable. Furthermore, in (Kolluri et al., 2017), a consensus-based power control law is designed on top of a primary angle droop[1] control layer. The approach presented in (Kolluri et al., 2017) is able to achieve frequency consensus and power sharing at steady-state. Recently, in (Kolluri et al., 2018), a modified frequency droop control scheme to address power sharing issues in the presence of clock drifts has been presented. However, the approaches proposed in (Kolluri et al., 2017, 2018) do not address the mandatory secondary frequency control objective, which is to restore the network frequency to the nominal value of 50 or 60 Hz.

A possible remedy to alleviate the impact of clock

[1] In contrast to the conventional frequency droop control law, in an angle droop controller, the voltage phase angle is calculated in proportion to the power injected by the inverter (Majumder et al., 2010).

drifts is to use a global time synchronization strategy (Guerrero et al., 2013), where a central unit communicates a global time signal to all the GFIs. Again, such a central setup increases the communication burden and is prone to single-point-failures. Another interesting option is to use clock synchronization protocols applied in sensor networks, see e.g., (Solis et al., 2006; Schenato and Fiorentin, 2011). Yet, when it comes to MGs, for implementing these clock synchronization protocols, an additional clock synchronization control has to be designed and should be activated before the primary and secondary controllers. Hence, adding such an additional control layer would increase the overall complexity of the hierarchical control architecture used in MGs (Guerrero et al., 2013).

1.2. Contributions

The main contributions of this paper are highlighted below.

1. We show that the most commonly employed distributed frequency controllers exhibit performance deteriorations in the presence of clock drifts.
2. Building upon the above observation, we propose a generalized distributed averaging integral (GDAI) control which at steady-state achieves secondary frequency control objectives in the presence of clock drifts. Furthermore, we derive a sufficient tuning criterion which guarantees that the closed-loop equilibrium point is locally asymptotically stable.
3. The performance of the GDAI controller in the presence of clock drifts is compared with two other distributed control approaches in the literature.

In contrast to (Kolluri et al., 2017; Martí et al., 2018; Kolluri et al., 2018), we neither linearize the electrical network, nor assume that the clock drift values are known (nor neglect their effect) in the stability analysis. Instead, we work with a non-linear MG model and consider the fact that clock drift values in practice are uncertain, but bounded. We use a Lyapunov function with classic kinetic and potential energy terms (Pai, 1989; Persis and Monshizadeh, 2017) to derive a stability criterion which can be verified without the knowledge of the operating point.

We present necessary and sufficient conditions for achieving accurate steady-state frequency restoration and power sharing in the presence of clock drifts with various distributed frequency controllers. The GDAI controller is proposed based on these necessary and sufficient conditions. Unfortunately, compared to an analysis assuming ideal clocks (Simpson-Porco et al., 2015; Bidram and Davoudi, 2012), the explicit consideration of clock drifts in the MG dynamics hampers the skew-symmetric interconnection with the GDAI controller and, hence, significantly complicates the derivation of controller parametrizations, which ensure closed-loop stability. This fact is addressed in the present paper by using a suitable Lyapunov function for the nonlinear MG dynamics, which permits to derive a sufficient stability criterion. The latter is cast as a set of LMIs, which can be efficiently solved using standard software like MATLAB® with Yalmip (Löfberg, 2004).

The present work extends our previous works in (Krishna et al., 2017, 2018) in the following sense. In this paper, the steady-state comparative study in (Krishna et al., 2017) and the tuning criterion in (Krishna et al., 2018) are unified with respect to a common MG model, hence making this paper self-contained. In addition, we provide an extensive numerical case study with comprehensive comparisons with other distributed control approaches in the literature.

The paper is organized as follows. In Section 2, we recall some preliminaries on graph theory and introduce the MG model. In Section 3, we introduce a general control representation of distributed secondary frequency controllers and derive sufficient conditions to achieve accurate frequency restoration and power sharing in the presence of clock drifts. Based on these conditions, we propose a GDAI control law which at steady-state achieves the aforementioned control objectives in the presence of clock drifts. In Section 4, a tuning criterion in the form of linear matrix inequalities (LMIs) which ensures robust stability of the closed-loop equilibrium point with GDAI control is presented. In Section 5, the performance of GDAI control is compared with other distributed approaches via simulation. Finally, we summarize our work and suggest some future research directions in Section 6.

2. Preliminaries

We denote by I_n the $n \times n$ identity matrix, by $\mathbb{0}_{n\times m}$ the $n\times m$ matrix with all entries equal to zero, by $\mathbb{1}_n$ the vector with all entries being equal to one and by $\mathbb{0}_n$ the zero vector. Furthermore, $\|\cdot\|_2$ denotes the Euclidean norm. Let F and H be two real symmetric matrices of same dimension. Then, the maximum eigenvalue F is denoted by $\lambda_{\max}(F)$ and the elements below the diagonal of F are denoted by $*$. If F is positive (negative) definite, we denote this by $F > 0$ ($F < 0$). If F is positive (negative) semidefinite, we denote this by $F \geq 0$ ($F \leq 0$). Similarly, $F > H$ and $F \geq H$ represent $F - H > 0$ and $F - H \geq 0$ respectively. Let $x = \mathrm{col}(x_i)$ denote a column vector with entries $x_i \in \mathbb{R}$, $Y = \mathrm{diag}(y_i)$ a diagonal matrix with diagonal entries $y_i \in \mathbb{R}$ and $X = \mathrm{blkdiag}(X_i)$

a block-diagonal matrix with matrix entries $X_i \in \mathbb{R}^{n_i \times n_i}$. Finally, for a function $f : \mathbb{R}^n \to \mathbb{R}$, ∇f denotes the gradient of f.

2.1. Algebraic graph theory

A weighted undirected graph of order $n > 1$ is a triple $\mathcal{G} = (\mathcal{N}, \mathcal{E}, \mathcal{W})$ with set of vertices $\mathcal{N} = \{1, \dots, n\}$. The set of edges is denoted by $\mathcal{E} \subseteq [\mathcal{N}]^2$, $\mathcal{E} = \{e_1, \dots, e_s\}$ where $s = |\mathcal{E}|$ and $[\mathcal{N}]^2$ represents the set of all two-element subsets of $\mathcal{N}$. Furthermore, $\mathcal{W} : \mathcal{E} \to \mathbb{R}_{>0}$ is a weight function. By assigning a random orientation to the edges, the incidence matrix $\mathcal{B} \in \mathbb{R}^{n \times s}$ can be defined element-wise as $h_{jl} = 1$ if node j is the source of the l-th edge e_l, $h_{jl} = -1$ if node j is the sink of the l-th edge e_l and $h_{jl} = 0$ otherwise. Then, the Laplacian matrix of the undirected weighted graph $\mathcal{G}$ is given by $\mathcal{L}_C = \mathcal{B}\mathbf{W}\mathcal{B}^\top$ where $\mathbf{W} = \mathrm{diag}(w_l) \in \mathbb{R}^{s \times s}$ and $w_l > 0$ is the weight of the l-the edge, $l = \{1, \dots, s\}$. A path is an ordered sequence of nodes such that any pair of consecutive nodes in the sequence is connected by an edge. The graph $\mathcal{G}$ is called connected if there exists a path between every pair of distinct nodes. The matrix $\mathcal{L}_C$ has a simple zero eigenvalue if and only if $\mathcal{G}$ is connected. Then, a corresponding right eigenvector is $\mathbb{1}_n$, i.e., $\mathcal{L}_C \mathbb{1}_n = \mathbb{0}_n$, yielding $\mathcal{L}_C \geq 0$. The reader is referred to (Godsil and Royle, 2001; Mesbahi and Egerstedt, 2010; Diestel, 2010) for more details on graph theory.

2.2. Primary droop-controlled MG model with clock drifts

We consider a Kron-reduced representation (Kundur, 1994) of an inverter-based MG and denote its set of network nodes by $\mathcal{N} = \{1, ..., n\}$, $n > 1$. As customary in secondary frequency control design, we assume that all voltage amplitudes are constant and that the line admittances are purely inductive (Kundur, 1994). The latter assumption is generally satisfied for MGs in which the inductive output impedance of the converter filter and/or transformer dominates the resistive part of the line impedances (Schiffer et al., 2014), and we only consider such MGs. Thus, if there is a power line between nodes $i \in \mathcal{N}$ and $k \in \mathcal{N}$, then this is represented by a nonzero susceptance $B_{ik} \in \mathbb{R}_{<0}$. Furthermore, the electrical network is assumed to be connected and the set of neighboring nodes of the i-th node is denoted by $\mathcal{N}_i = \{k \in \mathcal{N} \,|\, B_{ik} \neq 0\}$. The phase angle and voltage magnitude at each bus $i \in \mathcal{N}$ are denoted by $\delta_i : \mathbb{R}_{\geq 0} \to \mathbb{R}$, respectively $V_i \in \mathbb{R}_{>0}$. Note that voltage magnitudes are assumed to be constant. In this work we focus solely on aspects related to *frequency control in MGs* in the presence of clock drifts. In frequency-related studies in power systems, the assumption of constant voltage amplitudes is often made, see e.g., (Simpson-Porco et al., 2013; Schiffer et al., 2017a).

Under the explicit consideration of clock drifts, the model of a GFI connected at the i-th node, $i \in \mathcal{N}$ can be modeled as an AC voltage source given by (Schiffer et al., 2017b, 2015)

$$(1 + \mu_i)\dot{\delta}_i = u_i^\delta, \tag{2.1}$$

where $u_i^\delta : \mathbb{R}_{\geq 0} \to \mathbb{R}$ is the primary control input and $\mu_i \in \mathbb{R}$ is the constant, but uncertain relative drift of the clock of the i-th unit.

Following standard practice (Chandorkar et al., 1993; Guerrero et al., 2013), we assume that u_i^δ is obtained by the standard frequency droop control law given by

$$u_i^\delta = \omega^d - k_{P_i}(P_i^m - P_i^d), \tag{2.2}$$

where $\omega^d \in \mathbb{R}_{>0}$ is the desired electrical frequency, $k_{P_i} \in \mathbb{R}_{>0}$ is the droop coefficient, $P_i^d \in \mathbb{R}$ is the desired active power set point and $P_i^m : \mathbb{R}_{\geq 0} \to \mathbb{R}$ is the active power measured using a first order low pass filter given by

$$(1 + \mu_i)\tau_{P_i}\dot{P}_i^m = -P_i^m + P_i(\delta) + G_{ii}V_i^2, \tag{2.3}$$

where $\tau_{P_i} \in \mathbb{R}_{>0}$ is the time constant of the low pass filter and $G_{ii}V_i^2 \in \mathbb{R}_{\geq 0}$ represents the constant impedance load connected at the i-th node. The active power flow $P_i : \mathbb{R}^n \to \mathbb{R}$ at the i-th node is given by (Kundur, 1994)

$$P_i(\delta) = \sum\nolimits_{k \in \mathcal{N}_i} |B_{ik}| V_i V_k \sin(\delta_i - \delta_k), \tag{2.4}$$

where $\delta = \mathrm{col}(\delta_i) \in \mathbb{R}^n$ is the vector of phase angles.

Due to the consideration of clock drifts, it is convenient to introduce the *internal* frequency $\bar{\omega}_i : \mathbb{R}_{\geq 0} \to \mathbb{R}_{>0}$ of the inverter at the i-th node which is related to the actual *electrical* frequency $\omega_i = \dot{\delta}_i$ by (Schiffer et al., 2017b, 2015)

$$\bar{\omega}_i = (1 + \mu_i)\dot{\delta}_i = (1 + \mu_i)\omega_i, \quad \forall i \in \mathcal{N}. \tag{2.5}$$

In the literature, the effect of clock drifts is often neglected, i.e., it is assumed that $\mu_i = 0$ and $\bar{\omega}_i = \omega_i$. For example, see (Bidram et al., 2014; Simpson-Porco et al., 2015; Zhao et al., 2015; Schiffer et al., 2017a; Fu et al., 2016; Persis et al., 2016). In practice, the above assumption is not satisfied in inverter-based MGs (Schiffer et al., 2017b).

Furthermore, combining (2.1), (2.2) and (2.3) and recalling (2.5) yields the dynamics of a primary droop-controlled unit as

$$\begin{aligned} (1 + \mu_i)\dot{\delta}_i = \bar{\omega}_i &= \omega^d - k_{P_i}(P_i^m - P_i^d), \\ (1 + \mu_i)\tau_{P_i}\dot{P}_i^m &= -P_i^m + P_i(\delta) + G_{ii}V_i^2. \end{aligned} \tag{2.6}$$

For the presentation of our results, it is convenient to rewrite the dynamics (2.6) as follows. Differentiating the first equation in (2.6) with respect to time yields

$$\dot{\bar{\omega}}_i = -k_{P_i}\dot{P}_i^m = -k_{P_i}\frac{1}{(1+\mu_i)\tau_{P_i}}\left(-P_i^m + P_i(\delta) + G_{ii}V_i^2\right), \tag{2.7}$$

where to write the second equality, we have used the second equation in (2.6). Next, from the first equation in (2.6), the measured power P_i^m can be expressed as

$$P_i^m = \frac{1}{k_{P_i}}\left(-\bar{\omega}_i + \omega^d\right) + P_i^d. \tag{2.8}$$

Substituting (2.8) in (2.7) and multiplying the result with $1/k_{P_i}$ yields

$$(1+\mu_i)M_i\dot{\bar{\omega}}_i = -D_i(\bar{\omega}_i - \omega^d) - \left(P_i(\delta) + G_{ii}V_i^2 - P_i^d\right), \tag{2.9}$$

where $M_i = \tau_{P_i}/k_{P_i} \in \mathbb{R}_{>0}$ is the virtual inertia coefficient and $D_i = 1/k_{P_i} \in \mathbb{R}_{>0}$ is the damping coefficient.

Combining (2.9) with (2.5) yields

$$\begin{aligned}(1+\mu_i)\dot{\delta}_i &= \bar{\omega}_i,\\ (1+\mu_i)M_i\dot{\bar{\omega}}_i &= -D_i(\bar{\omega}_i - \omega^d) - \left(P_i(\delta) + G_{ii}V_i^2 - P_i^d\right),\end{aligned} \tag{2.10}$$

which is an equivalent representation of (2.6).

To derive a compact model representation of the MG, it is convenient to introduce the matrices

$$\begin{aligned}M &= \mathrm{diag}(M_i) \in \mathbb{R}^{n\times n}, D = \mathrm{diag}(D_i) \in \mathbb{R}^{n\times n},\\ \mu &= \mathrm{diag}(\mu_i) \in \mathbb{R}^{n\times n},\end{aligned}$$

and the vectors

$$\begin{aligned}\omega &= \mathrm{col}(\omega_i) \in \mathbb{R}^n,\ \bar{\omega} = \mathrm{col}(\bar{\omega}_i) \in \mathbb{R}^n,\\ P^{\mathrm{net}} &= \mathrm{col}(P_i^d - G_{ii}V_i^2) \in \mathbb{R}^n.\end{aligned}$$

Also, we introduce the *potential function* $U : \mathbb{R}^n \to \mathbb{R}$,

$$U(\delta) = -\sum\nolimits_{\{i,k\}\in[\mathcal{N}]^2} |B_{ik}|V_iV_k\cos(\delta_{ik}), \tag{2.11}$$

where we use the short-hand $\delta_{ik} = \delta_i - \delta_k$. Let $P(\delta) = \mathrm{col}(P_i(\delta)) \in \mathbb{R}^n$ be the vector of active power flows where $P_i(\delta)$ is defined in (2.4). With $U(\delta)$ defined in (2.11), we note that

$$\nabla_\delta U(\delta) = P(\delta).$$

Then, the dynamics (2.10) for the whole MG can be expressed as

$$\begin{aligned}(I_n+\mu)\dot{\delta} &= \bar{\omega},\\ (I_n+\mu)M\dot{\bar{\omega}} &= -D(\bar{\omega} - \mathbb{1}_n\omega^d) - \left(\nabla_\delta U(\delta) - P^{\mathrm{net}}\right).\end{aligned} \tag{2.12}$$

Observe that due to the skew symmetry of the power flows,

$$\mathbb{1}_n^\top \nabla_\delta U(\delta) = 0. \tag{2.13}$$

In MGs, sharing the active power injections in a fair manner is a practically important control objective (Schiffer, 2015; Guerrero et al., 2013). For this purpose, we recall the following definition (Schiffer et al., 2014; Dörfler et al., 2016).

Definition 2.1. *The active power injections are shared proportionally if*

$$\mathcal{X}\left(\nabla_\delta U(\delta^s) - P^{net}\right) = \alpha\mathbb{1}_n, \tag{2.14}$$

where $\alpha \in \mathbb{R}$, $\mathcal{X} = diag(\mathcal{X}_i) \in \mathbb{R}^{n\times n}$ is a weighting matrix with $\mathcal{X}_i \in \mathbb{R}_{>0}$ and $\nabla_\delta U(\delta^s) = \nabla_\delta U(\delta)|_{\delta=\delta^s} = P(\delta^s)$ is the vector of steady-state power flows.

Note that the parameter $\mathcal{X}_i$ is usually specified by the designer. A typically choice would be to select $\mathcal{X}_i = 1/S_i^N$ where S_i^N is the power rating of the i-th unit. Hence, achieving (2.14) at steady-state ensures that the loads connected in the MG are shared among the GFIs in a fair manner, i.e., in proportion to their power ratings. Furthermore, for the purpose of attaining steady-state power sharing, it has been shown in (Simpson-Porco et al., 2013, Theorem 7), (Schiffer et al., 2014, Lemma 6.2) that the entries of the damping matrix D in (2.12) can be chosen according to

$$\mathcal{X}D = \kappa I_n, \tag{2.15}$$

where $\kappa \in \mathbb{R}_{>0}$. Recall that D is the inverse droop coefficient matrix. Therefore, the condition (2.15) can be understood as a proportional choice of droop coefficients in correspondence to the power ratings.

3. Secondary control in the presence of clock drifts

Like any power network, a MG is also designed to work very close to the nominal frequency value of 50 or 60 Hz (Kundur, 1994; Anderson and Fouad, 2002). However, the proportional nature of primary droop control dynamics leading to (2.12) results in steady-state frequency deviation. Therefore, following standard practice (Zhao et al., 2015; Schiffer et al., 2017a; Dörfler et al., 2016), a secondary control input $u = \mathrm{col}(u_i) : \mathbb{R}_{\geq 0} \to \mathbb{R}^n$ is introduced to the model (2.12) with the aim of correcting the steady-state frequency deviation. Thus, (2.12) becomes

$$\begin{aligned}(I_n+\mu)\dot{\delta} &= \bar{\omega},\\ (I_n+\mu)M\dot{\bar{\omega}} &= -D(\bar{\omega} - \mathbb{1}_n\omega^d) - \left(\nabla_\delta U(\delta) - P^{\mathrm{net}}\right) + u.\end{aligned} \tag{3.1}$$

Along any synchronized motion (i.e., a motion with constant electrical frequencies $\omega^s = \omega^* \mathbb{1}_n$ for $\omega^* \in \mathbb{R}_{>0}$, constant phase angle differences $\delta_i^s - \delta_k^s$ and constant secondary control input u^s) of the system (3.1), we have that

$$\mathbb{1}_n^\top M(I_n + \mu)\dot{\bar{\omega}} = 0 = -\mathbb{1}_n^\top D(\bar{\omega}^s - \mathbb{1}_n \omega^d) - \mathbb{1}_n^\top \left(\nabla_\delta U(\delta^s) - P^{\text{net}}\right) + \mathbb{1}_n^\top u^s. \tag{3.2}$$

Note that in the presence of clock drifts, the internal frequencies are not uniform, i.e., from (2.5), $\omega^s = \omega^* \mathbb{1}_n$ implies that

$$\bar{\omega}^s = (I_n + \mu)\omega^s = \omega^*(I_n + \mu)\mathbb{1}_n. \tag{3.3}$$

Moreover, with (2.13), the scalar ω^* can be obtained from (3.2) as

$$\omega^* = \omega^d \frac{\mathbb{1}_n^\top D \mathbb{1}_n}{\mathbb{1}_n^\top D(I_n + \mu)\mathbb{1}_n} + \frac{\mathbb{1}_n^\top (P^{\text{net}} + u^s)}{\mathbb{1}_n^\top D(I_n + \mu)\mathbb{1}_n}. \tag{3.4}$$

From (3.4), it is obvious that $\omega^* = \omega^d$ only if u^s satisfies

$$\boxed{\mathbb{1}_n^\top (P^{\text{net}} + u^s) = \omega^d \mathbb{1}_n^\top D \mu \mathbb{1}_n.} \tag{3.5}$$

Remark 3.1. *In the case of ideal clocks, i.e., if $\mu = \mathbb{0}_{n\times n}$, from* (3.4)*, it is clear that if u^s satisfies $\mathbb{1}_n^\top (P^{net} + u^s) = 0$, we have $\omega^* = \omega^d$. Similar results assuming ideal inverter clocks have been presented in (Schiffer et al., 2017a; Zhao et al., 2015). However, in the presence of clock drifts ($\mu_i \neq 0$), satisfying $\mathbb{1}_n^\top (P^{net} + u^s) = 0$ does not guarantee $\omega^* = \omega^d$. See* (3.4)*.*

3.1. General distributed control representation

We are interested in designing a control law for u in (3.1) such that $\omega^* = \omega^d$ and power sharing, i.e., (2.14) are satisfied at steady-state. For this purpose, we propose the following *general distributed control representation* to study the effect of clock drifts on secondary frequency control,

$$\boxed{\begin{aligned} u &= p, \\ (I_n + \mu)\dot{p} &= -(\mathbf{B} + \beta \mathcal{X} \mathbf{D} \mathcal{L}_C)(\bar{\omega} - \mathbb{1}_n \omega^d) - \mathbf{D} \mathcal{X} \mathcal{L}_C \mathcal{X} p, \end{aligned}} \tag{3.6}$$

where $\mathbf{B} \in \mathbb{R}^{n\times n}$ and $\mathbf{D} \in \mathbb{R}^{n\times n}$ are diagonal controller matrices, $\beta \in \mathbb{R}$ is a controller parameter, $\mathcal{L}_C \in \mathbb{R}^{n\times n}$ is the Laplacian matrix representing the communication network and $\mathcal{X}$ is the design parameter defined in (2.14). The matrix $\mathbf{B}$ is commonly called the *pinning gain matrix*, see e.g. (Bidram et al., 2014).

It is customary to use the internal frequency of the inverter to implement a distributed control law like (3.6), since it obviates the requirement for extra frequency measurement. This is mainly because extra measurement devices can potentially increase the complexity and can bring in further measurement errors into the system. For example, see (Bidram et al., 2014; Simpson-Porco et al., 2015; Schiffer et al., 2017a; Schiffer and Dörfler, 2016; Zhao et al., 2015). Therefore, it is important to note that in the control law (3.6), we use the internal frequency $\bar{\omega}$. However, in the works mentioned above, the authors do not consider clock drifts and assume that the internal frequency and the electrical frequency are the same, i.e., $\bar{\omega} = \omega$, see (3.3). Yet, when explicitly considering clock drifts, from (2.5), it is relevant to note that $\bar{\omega} = (I_n + \mu)\omega$.

The control law (3.6) represents a generalized version of various distributed secondary frequency controllers and can be parametrized as follows.

DAI control

The DAI control presented/studied in (Simpson-Porco et al., 2015; Schiffer et al., 2017a; Schiffer and Dörfler, 2016; Zhao et al., 2015) can be obtained from (3.6) if the control parameters in (3.6) are chosen such that

$$\mathbf{B} > 0, \beta = 0, \mathbf{D} > 0. \tag{3.7}$$

By using (3.7) in (3.6) yields the DAI control (Simpson-Porco et al., 2015, Eq. 6)

$$\boxed{\begin{aligned} u &= p, \\ (I_n + \mu)\dot{p} &= -\mathbf{B}(\bar{\omega} - \mathbb{1}_n \omega^d) - \mathbf{D} \mathcal{X} \mathcal{L}_C \mathcal{X} p, \end{aligned}} \tag{3.8}$$

where $\mathbf{B} > 0$ and $\mathbf{D} > 0$.

Pinning control

The pinning control law proposed in (Bidram et al., 2014) can be obtained from (3.6) if the control parameters in (3.6) are chosen such that

$$\mathbf{B} \geq 0, \beta = 0, \mathbf{D} > 0. \tag{3.9}$$

Thus, (3.6), (3.9) yields the pinning control (Bidram et al., 2014, Eq. 52,53)

$$\boxed{\begin{aligned} u &= p, \\ (I_n + \mu)\dot{p} &= -\mathbf{B}(\bar{\omega} - \mathbb{1}_n \omega^d) - \mathbf{D} \mathcal{X} \mathcal{L}_C \mathcal{X} p, \end{aligned}} \tag{3.10}$$

where $\mathbf{B} \geq 0$ and $\mathbf{D} > 0$. The correspondence of the pinning control law presented in (Bidram et al., 2014, Eq. 52,53) with that of (3.10) is detailed in the appendix.

For the subsequent analysis, to represent the natural power-balance of the system (3.1), (3.6), it is convenient to introduce the notion below.

Definition 3.2 (Synchronized motion)**.** *The closed-loop system* (3.1)*,* (3.6) *admits a synchronized motion if it has a solution for all* $t \geq 0$ *of the form*

$$\delta^s(t) = \delta_0^s + \omega^* \mathbb{1}_n t, \quad \omega^s(t) = \omega^* \mathbb{1}_n, \quad p^s(t) \in \mathbb{R}^n,$$

where $\omega^* \in \mathbb{R}_{>0}$ *is the synchronized electrical frequency and* $\delta_0^s \in \mathbb{R}^n$ *such that*

$$|\delta_{0,i}^s - \delta_{0,k}^s| < \frac{\pi}{2} \quad \forall i \in \mathcal{N},\ \forall k \in \mathcal{N}_i.$$

In Definition 3.2, $|\delta_{0,i}^s - \delta_{0,k}^s| < \frac{\pi}{2}$ limits the power flow within the desired power-angle stability region (Machowski et al., 2008, Chapter 5) over the line connecting i-th and k-th units. Furthermore, the terminology *synchronized motion* denotes the fact that with constant phase angle differences $\delta_i^s(t) - \delta_j^s(t)$ for all $t \geq 0$, $i, j \in \mathcal{N}$ in the system (3.1), (3.6) imply that the frequencies of all the units have converged to a common value, i.e., $\dot{\delta}_i^s = \dot{\delta}_i^s = \omega^*$, $\omega^* \in \mathbb{R}_{>0}$. Moreover, note that there is no unique synchronized motion of the system (3.1), (3.6) with the power flow given by (2.4), but any motion with $\omega^s(t)$ and $p^s(t)$ given in Definition 3.2 and with $\delta^s(t) = \delta_0^s + \omega^* \mathbb{1}_n t + \alpha \mathbb{1}_n$ for any $\alpha \in \mathbb{R}$ is a desired synchronized motion, see also (Schiffer et al., 2014, Remark 5.7). For further details about synchronized motions in power system models similar to (3.1), (3.6), the reader is referred to (Schiffer and Dörfler, 2016, Lemma 4.2). We make the following power-balance feasibility assumption.

Assumption 3.3. *The closed-loop system* (3.1)*,* (3.6) *possesses a synchronized motion.* □

In practice, clock drift values observed in commercial inverters can vary from 1 μsec (Schiffer et al., 2017b; Anritsu, 2001) to 1 millisec (Kolluri et al., 2017, Table I) depending on the quality of the micro-controller used. Thus, as outlined in (Schiffer et al., 2017b, 2015) for the purpose of secondary frequency control, it is reasonable to assume that the clock drifts are bounded. This is formalized in the assumption below.

Assumption 3.4. $\|\mu\|_2 \leq \epsilon, \quad 0 \leq \epsilon < 1.$

We are interested in the following problem.

Problem 3.5 (**Secondary control objectives**)**.** *Consider the closed-loop system* (3.1)*,* (3.6) *with Assumption 3.4 and Assumption 3.3. Design the parameters* $\mathbf{B}$*,* β*,* $\mathbf{D}$ *and edge-weights of* $\mathcal{L}_C$ *in* (3.1)*,* (3.6) *such that the following control objectives are satisfied:*

1. *Accurate frequency restoration at steady-state, that is,*
$$\omega^* = \omega^d. \tag{3.11}$$
2. *Steady-state power sharing according to Definition 2.1.*
3. *Asymptotic convergence of the solutions of the system* (3.1)*,* (3.6) *to the synchronized motion in Definition 3.2.*

3.2. Steady-state performance

In this section, we address the first two points in Problem 3.5. We begin by providing necessary and sufficient conditions with which the first objective in Problem 3.5 can be accomplished.

Lemma 3.6 (Accurate frequency restoration)**.** *Consider the closed-loop system* (3.1)*,* (3.6) *with Assumption 3.3. Let* $\mathbf{D} > 0$*. Suppose that the diagonal matrix* $\mathbf{B}$ *has at least one positive entry. Then, the synchronized electrical frequency of the system* (3.1)*,* (3.6) *is given by*

$$\omega^* = \frac{\mathbb{1}_n^\top \mathbf{D}^{-1} \mathcal{X}^{-1} \mathbf{B} \mathbb{1}_n}{\mathbb{1}_n^\top \mathbf{D}^{-1} \mathcal{X}^{-1} \mathbf{B} (I_n + \mu) \mathbb{1}_n} \omega^d. \tag{3.12}$$

Furthermore, (3.11) *is satisfied if and only if*

$$\mathbb{1}_n^\top \mathbf{D}^{-1} \mathcal{X}^{-1} \mathbf{B} \mu \mathbb{1}_n = 0. \tag{3.13}$$

Proof. Along any synchronized motion, the electrical frequencies at all nodes of (3.1), (3.6) have to be identical, i.e.,

$$\dot{\delta}^s = \omega^s = \mathbb{1}_n \omega^*, \tag{3.14}$$

which directly implies (3.3). Furthermore, at steady-state, $\dot{p}^s = \mathbb{0}_n$. Hence, (3.6) becomes

$$-(I_n + \mu)\dot{p}^s = \mathbb{0}_n = (\mathbf{B} + \beta \mathcal{X} \mathbf{D} \mathcal{L}_C)(\bar{\omega}^s - \mathbb{1}_n \omega^d) + \mathbf{D} \mathcal{X} \mathcal{L}_C \mathcal{X} p^s. \tag{3.15}$$

Multiplying (3.15) from the left with $\mathbb{1}_n^\top \mathbf{D}^{-1} \mathcal{X}^{-1}$ and recalling the fact that $\mathbb{1}_n^\top \mathcal{L}_C = \mathbb{0}_n^\top$, yields

$$0 = \mathbb{1}_n^\top \mathbf{D}^{-1} \mathcal{X}^{-1} \mathbf{B} (\bar{\omega}^s - \mathbb{1}_n \omega^d).$$

Using (3.3) in the above equation leads to

$$0 = \mathbb{1}_n^\top \mathbf{D}^{-1} \mathcal{X}^{-1} \mathbf{B} \left((I_n + \mu) \mathbb{1}_n \omega^* - \mathbb{1}_n \omega^d \right). \tag{3.16}$$

Under the standing assumption that at least one entry of the diagonal matrix $\mathbf{B}$ is positive, ω^* can be solved from (3.16) yielding (3.12).

Furthermore, from (3.12), we note that $\omega^* = \omega^d$ if and only if

$$\mathbb{1}_n^\top \mathbf{D}^{-1} \mathcal{X}^{-1} \mathbf{B} (I_n + \mu) \mathbb{1}_n = \mathbb{1}_n^\top \mathbf{D}^{-1} \mathcal{X}^{-1} \mathbf{B} \mathbb{1}_n,$$

which is equivalent to (3.13), completing the proof. □

In the following lemma, we present necessary and sufficient conditions under which the second objective in Problem 3.5 can be fulfilled.

Lemma 3.7 (Power sharing)**.** *Consider the closed-loop system* (3.1)*,* (3.6) *with Assumption 3.3. Let* $\mathbf{D} > 0$*. Suppose that the diagonal matrix* $\mathbf{B}$ *has at least one positive entry. Then, active power sharing according to Definition 2.1 along the synchronized motion is achieved if and only if* $\mathbf{B}$*,* β*,* $\mathbf{D}$ *and* $\mathcal{L}_C$ *are chosen such that*

$$[\mathbf{D}^{-1}\mathcal{X}^{-1}\mathbf{B} + (\beta+\kappa)\mathcal{L}_C]\mathbf{F}\mathbb{1}_n\omega^d = \mathbb{0}_n, \tag{3.17}$$

where

$$\mathbf{F} = \frac{\mathbb{1}_n^\top \mathbf{D}^{-1}\mathcal{X}^{-1}\mathbf{B}\mathbb{1}_n}{\mathbb{1}_n^\top \mathbf{D}^{-1}\mathcal{X}^{-1}\mathbf{B}(I_n+\mu)\mathbb{1}_n}(I_n+\mu) - I_n. \tag{3.18}$$

Proof. Along a synchronized motion, the primary control dynamics (3.1) with $u = p$ becomes

$$\mathbb{0}_n = -D(\bar{\omega}^s - \mathbb{1}_n\omega^d) - \left(\nabla_\delta U(\delta^s) - P^{\text{net}}\right) + p^s. \tag{3.19}$$

We can rearrange (3.19) as

$$p^s = D(\bar{\omega}^s - \mathbb{1}_n\omega^d) + \left(\nabla_\delta U(\delta^s) - P^{\text{net}}\right). \tag{3.20}$$

Next, consider (3.6) at steady-state given by

$$\mathbb{0}_n = (\mathbf{B} + \beta\mathcal{X}\mathbf{D}\mathcal{L}_C)(\bar{\omega}^s - \mathbb{1}_n\omega^d) + \mathbf{D}\mathcal{X}\mathcal{L}_C\mathcal{X}p^s. \tag{3.21}$$

Inserting p^s obtained from (3.20) in (3.21) results in

$$\begin{aligned}\mathbb{0}_n = {} & (\mathbf{B} + \beta\mathcal{X}\mathbf{D}\mathcal{L}_C)(\bar{\omega}^s - \mathbb{1}_n\omega^d) + \mathbf{D}\mathcal{X}\mathcal{L}_C\mathcal{X}D(\bar{\omega}^s - \mathbb{1}_n\omega^d) \\ & + \mathbf{D}\mathcal{X}\mathcal{L}_C\mathcal{X}\left(\nabla_\delta U(\delta^s) - P^{\text{net}}\right).\end{aligned}$$

Under the standing assumption that (2.15) is satisfied, the above equation becomes

$$\begin{aligned}\mathbb{0}_n = {} & (\mathbf{B} + \beta\mathcal{X}\mathbf{D}\mathcal{L}_C + \kappa\mathbf{D}\mathcal{X}\mathcal{L}_C)(\bar{\omega}^s - \mathbb{1}_n\omega^d) \\ & + \mathbf{D}\mathcal{X}\mathcal{L}_C\mathcal{X}\left(\nabla_\delta U(\delta^s) - P^{\text{net}}\right),\end{aligned}$$

which, when left-multiplied with $\mathbf{D}^{-1}\mathcal{X}^{-1} > 0$, yields

$$\begin{aligned}\mathbb{0}_n = {} & (\mathbf{D}^{-1}\mathcal{X}^{-1}\mathbf{B} + \beta\mathcal{L}_C + \kappa\mathcal{L}_C)(\bar{\omega}^s - \mathbb{1}_n\omega^d) \\ & + \mathcal{L}_C\mathcal{X}\left(\nabla_\delta U(\delta^s) - P^{\text{net}}\right).\end{aligned} \tag{3.22}$$

Recall that $\mathcal{L}_C$ is the Laplacian matrix of a connected undirected graph. Hence,

$$\mathcal{L}_C\mathcal{X}\left(\nabla_\delta U(\delta^s) - P^{\text{net}}\right) = \mathbb{0}_n$$

if and only if (2.14) is satisfied. From (3.22), $\mathcal{L}_C\mathcal{X}\left(\nabla_\delta U(\delta^s) - P^{\text{net}}\right) = \mathbb{0}_n$ if and only if

$$(\mathbf{D}^{-1}\mathcal{X}^{-1}\mathbf{B} + (\beta+\kappa)\mathcal{L}_C)(\bar{\omega}^s - \mathbb{1}_n\omega^d) = \mathbb{0}_n. \tag{3.23}$$

Finally, with (3.3) and ω^* given by (3.12), the condition (3.23) holds if and only if (3.17) is satisfied. This completes the proof. □

In the presence of clock drifts, it is straightforward to verify that the DAI parametrization (3.7) neither satisfies Lemma 3.6 nor Lemma 3.7. Turning to the pinning parametrization (3.9), we see that (3.9) satisfies the conditions of Lemma 3.6 if the structure of the pinning gain matrix $\mathbf{B}$ is chosen such that $\mathbf{B}\mu = \mathbb{0}_{n\times n}$. However, the parametrization (3.9) does not satisfy Lemma 3.7.

We are interested in finding parameters of the controller (3.6) which satisfy both Lemma 3.6 and Lemma 3.7. But, since the coefficients μ_i are unknown and different for different units, Lemma 3.7 reveals that unlike in the case of ideal clocks (Bidram et al., 2014; Simpson-Porco et al., 2015; Schiffer et al., 2017a; Fu et al., 2016; Persis et al., 2016), when taking clock drifts explicitly into account, it is hard to determine $\mathbf{B}$, β and $\mathbf{D}$ directly from the conditions presented in Lemmata 3.6 and 3.7. Therefore, instead, below we present a sufficient condition for the control parameters $\mathbf{B}$, β and $\mathbf{D}$ such that Lemmata 3.6 and 3.7 are satisfied.

Lemma 3.8 (Accurate frequency restoration and power sharing)**.** *Consider the closed-loop system* (3.1)*,* (3.6) *with Assumption 3.3. Let* $\mathbf{D} > 0$*. Suppose that the diagonal matrix* $\mathbf{B}$ *has at least one positive entry. Then, the first two objectives in Problem 3.5 along a synchronized motion are achieved if the control parameters* $\mathbf{B}$ *and* β *are chosen such that*

$$\mathbf{B}\mu = \mathbb{0}_{n\times n}, \text{ and } \beta = -\kappa. \tag{3.24}$$

Proof. Consider Lemma 3.6. For $\mathbf{B}\mu = \mathbb{0}_{n\times n}$, (3.13) holds. Thus, we have (3.11).

Next, consider Lemma 3.7. With $\mathbf{B}\mu = \mathbb{0}_{n\times n}$, (3.17) becomes

$$[(\beta+\kappa)\mathcal{L}_C]\mu\mathbb{1}_n\omega^d = \mathbb{0}_n,$$

which holds when $\beta = -\kappa$. Hence, Lemma 3.7 is satisfied, yielding steady-state power sharing (2.14). This completes the proof. □

The condition $\mathbf{B}\mu = \mathbb{0}_{n\times n}$ presented in Lemma 3.8 can be interpreted as follows. Define the clock of one of the units in the network as master clock, say the k-th unit, $k \geq 1$. Then, $\mu_k = 0$ and the drifts $\mu_i, i \neq k$, of all other clocks in the MG are expressed with respect to the master clock of the k-th unit. Furthermore, the diagonal pinning gain matrix $\mathbf{B} \geq 0$ will have a non-zero positive entry only at the (k,k)-th position resulting in $\mathbf{B}\mu = \mathbb{0}_{n\times n}$.

Applying the parametrization (3.24) to the general

control representation (3.6) yields

$$\boxed{\begin{aligned} u &= p, \\ (I_n+\mu)\dot{p} &= (-\mathbf{B}+\kappa\mathcal{X}\mathbf{D}\mathcal{L}_C)(\bar{\omega}-\mathbb{1}_n\omega^d)-\mathbf{D}\mathcal{X}\mathcal{L}_C\mathcal{X}p, \end{aligned}} \tag{3.25}$$

with $\mathbf{B}\mu = \mathbb{0}_{n\times n}, \mathbf{B} \geq 0$. The control law (3.25) is termed generalized distributed averaging integral (GDAI) control in the remainder of this paper.

4. Robust GDAI control design

We have identified that the GDAI controller given by (3.25) achieves the first two objectives mentioned in Problem 3.5. In this section, the third point in Problem 3.5 is addressed. More precisely, a sufficient tuning criterion with which the solutions of the system (3.1), (3.25) asymptotically converge to the synchronized motion in Definition 3.2 is presented.

4.1. Coordinate reduction and error states

Combining (3.1) and (3.25) yields the closed-loop system

$$\begin{aligned} (I_n+\mu)\dot{\delta} &= \bar{\omega}, \\ (I_n+\mu)M\dot{\bar{\omega}} &= -D(\bar{\omega}-\mathbb{1}_n\omega^d)-\left(\nabla_\delta U(\delta)-P^{\text{net}}\right)+p, \\ (I_n+\mu)\dot{p} &= (-\mathbf{B}+\kappa\mathcal{X}\mathbf{D}\mathcal{L}_C)(\bar{\omega}-\mathbb{1}_n\omega^d)-\mathbf{D}\mathcal{X}\mathcal{L}_C\mathcal{X}p. \end{aligned} \tag{4.1}$$

As the power flow $\nabla_\delta U(\delta)$ only depends on angle differences (see (2.4)), following (Schiffer et al., 2014) we choose an arbitrary node, say node n, and express all angles relative to that node, i.e.,

$$\theta = \mathcal{R}^\top\delta, \quad \theta\in\mathbb{R}^{n-1}, \quad \mathcal{R} = \begin{bmatrix} I_{n-1} \\ -\mathbb{1}_{n-1}^\top \end{bmatrix} \in \mathbb{R}^{n\times(n-1)}.$$

Note that the matrix $\mathcal{R}$ has the property that $\mathbb{1}_n^\top\mathcal{R} = \mathbb{0}_{n-1}^\top$.

Next, with Assumption 3.3 for the system (4.1), we introduce the error states

$$\begin{aligned} \tilde{\omega} &= \bar{\omega}-\bar{\omega}^s = \bar{\omega}-(I_n+\mu)\mathbb{1}_n\omega^d, \\ \tilde{\theta} &= \theta-\theta^s, \quad \tilde{p} = p-p^s, \quad x = \operatorname{col}\left(\tilde{\theta},\,\tilde{\omega},\,\tilde{p}\right), \end{aligned}$$

where we have used (3.3) and (3.11) to express $\bar{\omega}^s$.

Thus, the resulting error dynamics of the system (4.1) is given by

$$\begin{aligned} \dot{\tilde{\theta}} &= \mathcal{R}^\top(I_n+\mu)^{-1}\tilde{\omega}, \\ (I_n+\mu)M\dot{\tilde{\omega}} &= -D\tilde{\omega}-\mathcal{R}\left[\nabla_{\tilde{\theta}}U(\delta(\tilde{\theta}+\theta^s))-\nabla_{\tilde{\theta}}U(\delta(\theta^s))\right]+\tilde{p}, \\ (I_n+\mu)\dot{\tilde{p}} &= (-\mathbf{B}+\kappa\mathcal{X}\mathbf{D}\mathcal{L}_C)\tilde{\omega}-\mathbf{D}\mathcal{X}\mathcal{L}_C\mathcal{X}\tilde{p}, \end{aligned} \tag{4.2}$$

where

$$\begin{aligned} \nabla_{\tilde{\theta}}U(\delta(\tilde{\theta}+\theta^s)) &= \frac{\partial U(\delta(\tilde{\theta}+\theta^s))}{\partial\tilde{\theta}}, \\ \nabla_{\tilde{\theta}}U(\delta(\theta^s)) &= \frac{\partial U(\delta(\theta+\theta^s))}{\partial\tilde{\theta}}\Big|_{\tilde{\theta}=\mathbb{0}_{n-1}}. \end{aligned}$$

Note that $x^* = \mathbb{0}_{3n-1}$ is an equilibrium point of (4.2). Furthermore, asymptotic stability of $x^* = \mathbb{0}_{3n-1}$ implies asymptotic convergence of solutions of the system (4.1) to the synchronized motion in Definition 3.2 up to a uniform shift of all angles (Schiffer et al., 2014).

4.2. Stability criterion

For the presentation of our main result, it is convenient to define the following. Since μ is a diagonal matrix, with Assumption 3.4 we have that

$$\begin{aligned} \|\mu(I_n+\mu)^{-1}\|_2 &\leq g_1(\epsilon), \quad g_1(\epsilon) = \tfrac{\epsilon}{1-\epsilon} > 0, \\ \|(\mu^2+2\mu)(I_n+\mu)^{-2}\|_2 &\leq g_2(\epsilon), \quad g_2(\epsilon) = \tfrac{\epsilon^2+2\epsilon}{(1-\epsilon)^2} > 0. \end{aligned} \tag{4.3}$$

Moreover, we define the matrices

$$\begin{aligned} T &:= \begin{bmatrix} T_{11} & \frac{1}{2}\left(-\varsigma I_n-\sigma D\mathbb{1}_n\mathbb{1}_n^\top\mathbf{D}^{-1}\mathcal{X}^{-1}+\tilde{\mathbf{B}}-\kappa\mathcal{L}_C\mathcal{X}\right) \\ * & T_{22} \end{bmatrix}, \\ \hat{T}_2 &:= \begin{bmatrix} \sigma M\mathbb{1}_n\mathbb{1}_n^\top\tilde{\mathbf{B}}\mathcal{X}^{-1} & \sigma\mathbf{D}^{-1}\mathcal{X}^{-1}\mathbb{1}_n\mathbb{1}_n^\top D \\ \mathbb{0}_{n\times n} & -\sigma\mathbf{D}^{-1}\mathcal{X}^{-1}\mathbb{1}_n\mathbb{1}_n^\top \end{bmatrix}, \\ H_\mu &:= \begin{bmatrix} \varsigma g_2(\epsilon)M & \mathbb{0}_{n\times n} \\ \mathbb{0}_{n\times n} & g_1(\epsilon)\mathbf{D}^{-1} \end{bmatrix}, \end{aligned} \tag{4.4}$$

where $g_1(\epsilon)$ and $g_2(\epsilon)$ are defined in (4.3). Furthermore, $\sigma\in\mathbb{R}_{>0}$, $\tilde{\mathbf{B}} = \mathbf{D}^{-1}\mathbf{B} \geq 0$ and

$$\begin{aligned} T_{11} &= \varsigma D-\frac{\sigma}{2}\left(M\mathbb{1}_n\mathbb{1}_n^\top\tilde{\mathbf{B}}\mathcal{X}^{-1}+\mathcal{X}^{-1}\tilde{\mathbf{B}}\mathbb{1}_n\mathbb{1}_n^\top M\right), \\ T_{22} &= \mathcal{X}\mathcal{L}_C\mathcal{X}+\frac{\sigma}{2}\left(\mathbf{D}^{-1}\mathcal{X}^{-1}\mathbb{1}_n\mathbb{1}_n^\top+\mathbb{1}_n\mathbb{1}_n^\top\mathcal{X}^{-1}\mathbf{D}^{-1}\right). \end{aligned}$$

The stability result is as follows.

Proposition 4.1. *Consider the system* (4.2) *with Assumption 3.3. Recall* $g_1(\epsilon)$ *and* $g_2(\epsilon)$ *defined in* (4.3). *Suppose that there exist* $\varsigma\in\mathbb{R}_{>0}$ *and* $\sigma\in\mathbb{R}_{>0}$, *such that*

$$H_{nom} := \begin{bmatrix} \varsigma M & -\sigma M\mathbb{1}_n\mathbb{1}_n^\top\mathbf{D}^{-1}\mathcal{X}^{-1} \\ * & \mathbf{D}^{-1} \end{bmatrix} > H_\mu, \tag{4.5}$$

and

$$\begin{aligned} T &> \left(\epsilon\zeta+\varsigma g_1(\epsilon)\sqrt{\lambda_{\max}(D^2)+1}\right)I_{2n}, \\ 0 &\geq \begin{bmatrix} -\zeta I_{2n} & \hat{T}_2 \\ * & -\zeta I_{2n} \end{bmatrix}, \end{aligned} \tag{4.6}$$

where $\zeta \in \mathbb{R}_{>0}$ and the matrices H_μ, T and $\hat{T}_2$ are defined in (4.4)*. Then, local asymptotic stability of $x^* = \mathbb{0}_{3n-1}$ is guaranteed for all unknown clock drifts satisfying Assumption 3.4.*

Proof. Consider the Lyapunov function candidate

$$\begin{aligned}\mathcal{V} = &\frac{\varsigma}{2}\tilde{\omega}^\top M\tilde{\omega} + \varsigma U(\delta(\tilde{\theta}+\theta^s)) - \varsigma\nabla_{\tilde{\theta}}U(\delta(\theta^s))^\top\tilde{\theta}\\ &+ \frac{1}{2}\tilde{p}^\top\mathbf{D}^{-1}(I_n+\mu)\tilde{p}\\ &- \sigma\tilde{p}^\top(I_n+\mu)\mathbf{D}^{-1}\mathcal{X}^{-1}\mathbb{1}_n\mathbb{1}_n^\top M(I_n+\mu)\tilde{\omega},\end{aligned} \tag{4.7}$$

where $\varsigma > 0$ and $\sigma > 0$ are design parameters. The Lyapunov function $\mathcal{V}$ contains kinetic and potential energy terms $\tilde{\omega}^\top M\tilde{\omega}$, respectively $U(\tilde{\theta})$ (Pai, 1989), a quadratic term in secondary control input $\tilde{p}$ and a cross term between $\tilde{\omega}$ and $\tilde{p}$ which allows us to ensure that $\mathcal{V}$ is decreasing along the trajectories of (4.2).

First, we will show that $\mathcal{V}$ is indeed positive definite under the premises of Proposition 4.1. Note that $\nabla_x\mathcal{V}\big|_{x^*} = \mathbb{0}_{3n-1}$. This shows that x^* is a critical point of $\mathcal{V}$. Moreover, the Hessian of $\mathcal{V}$ at x^* is given by

$$\nabla_x^2\mathcal{V}|_{x*} = \begin{bmatrix}\varsigma\nabla_{\tilde{\theta}}^2U(\delta(\tilde{\theta}+\theta^s))|_{\tilde{\theta}=\mathbb{0}_{n-1}} & \mathbb{0}_{(n-1)\times n} & \mathbb{0}_{(n-1)\times n}\\ * & \varsigma M & H_{23}\\ * & * & \mathbf{D}^{-1}(I_n+\mu)\end{bmatrix}, \tag{4.8}$$

where $H_{23} = -\sigma(I_n+\mu)M\mathbb{1}_n\mathbb{1}_n^\top\mathbf{D}^{-1}\mathcal{X}^{-1}(I_n+\mu)$. Note that $\nabla_{\tilde{\theta}}^2U(\delta(\tilde{\theta}+\theta^s))|_{\tilde{\theta}=\mathbb{0}_{n-1}} > 0$ (Schiffer et al., 2014, Lemma 5.8). Therefore, the Hessian $\nabla_x^2\mathcal{V}|_{x*}$ is positive definite if and only if

$$\begin{bmatrix}\varsigma M & -\sigma(I_n+\mu)M\mathbb{1}_n\mathbb{1}_n^\top\mathbf{D}^{-1}\mathcal{X}^{-1}(I_n+\mu)\\ * & \mathbf{D}^{-1}(I_n+\mu)\end{bmatrix} > 0. \tag{4.9}$$

By performing a congruence transformation using the positive definite matrix $S = \mathrm{blkdiag}\left((I_n+\mu)^{-1},(I_n+\mu)^{-1}\right)$ and by invoking Sylvester's law of inertia (Horn and Johnson, 2012), we see that the matrix on the left hand side of (4.9) is positive definite if and only if the following matrix inequality is satisfied

$$\begin{bmatrix}\varsigma(I_n+\mu)^{-2}M & -\sigma M\mathbb{1}_n\mathbb{1}_n^\top\mathbf{D}^{-1}\mathcal{X}^{-1}\\ * & (I_n+\mu)^{-1}\mathbf{D}^{-1}\end{bmatrix} > 0. \tag{4.10}$$

Inequality (4.10) can be written as

$$H_{\mathrm{nom}} - \begin{bmatrix}\varsigma(\mu^2+2\mu)(I_n+\mu)^{-2}M & \mathbb{0}_{n\times n}\\ \mathbb{0}_{n\times n} & \mu(I_n+\mu)^{-1}\mathbf{D}^{-1}\end{bmatrix} > 0,$$

where H_{nom} is defined in (4.5). Furthermore, since μ, M and $\mathbf{D}$ are all diagonal matrices, we have that

$$\begin{bmatrix}\varsigma(\mu^2+2\mu)(I_n+\mu)^{-2}M & \mathbb{0}_{n\times n}\\ \mathbb{0}_{n\times n} & \mu(I_n+\mu)^{-1}\mathbf{D}^{-1}\end{bmatrix} \leq H_\mu,$$

where H_μ is defined in (4.4). Consequently, under the premises of Proposition 4.1, $\nabla_x^2\mathcal{V}|_{x*} > 0$, confirming the positive definiteness of $\mathcal{V}$. Note that $\nabla_x\mathcal{V}\big|_{x^*} = \mathbb{0}_{3n-1}$ and $\nabla_x^2\mathcal{V}|_{x*} > 0$ implies that x^* is a strict local minimum of $\mathcal{V}$ (van der Schaft, 2000).

Next, we calculate the time derivative of $\mathcal{V}$ along the solutions of (4.2), which yields

$$\begin{aligned}\dot{\mathcal{V}} = &-\varsigma\tilde{\omega}^\top(I_n+\mu)^{-1}D\tilde{\omega} + \varsigma\tilde{\omega}^\top(I_n+\mu)^{-1}\tilde{p}\\ &+ \tilde{p}^\top\left(-\mathbf{D}^{-1}\mathbf{B} + \kappa\mathcal{X}\mathcal{L}_C\right)\tilde{\omega} - \tilde{p}^\top\mathcal{X}\mathcal{L}_C\mathcal{X}\tilde{p}\\ &+ \sigma\tilde{p}^\top(I_n+\mu)\mathbf{D}^{-1}\mathcal{X}^{-1}\mathbb{1}_n\mathbb{1}_n^\top D\tilde{\omega}\\ &- \sigma\tilde{p}^\top(I_n+\mu)\mathbf{D}^{-1}\mathcal{X}^{-1}\mathbb{1}_n\mathbb{1}_n^\top\tilde{p}\\ &+ \sigma\tilde{\omega}^\top(I_n+\mu)M\mathbb{1}_n\mathbb{1}_n^\top\mathcal{X}^{-1}\mathbf{D}^{-1}\mathbf{B}\tilde{\omega}\\ = &-\eta^\top\begin{bmatrix}\tilde{\mathbf{T}}_{11} & \tilde{\mathbf{T}}_{12}\\ \tilde{\mathbf{T}}_{21} & \tilde{\mathbf{T}}_{22}\end{bmatrix}\eta,\end{aligned} \tag{4.11}$$

where

$$\eta := \mathrm{col}(\tilde{\omega},\tilde{p}), \tag{4.12}$$

and

$$\begin{aligned}\tilde{\mathbf{T}}_{11} &= \varsigma(I_n+\mu)^{-1}D - \sigma(I_n+\mu)M\mathbb{1}_n\mathbb{1}_n^\top\mathcal{X}^{-1}\mathbf{D}^{-1}\mathbf{B},\\ \tilde{\mathbf{T}}_{22} &= \mathcal{X}\mathcal{L}_C\mathcal{X} + \sigma(I_n+\mu)\mathbf{D}^{-1}\mathcal{X}^{-1}\mathbb{1}_n\mathbb{1}_n^\top,\\ \tilde{\mathbf{T}}_{12} &= -\varsigma(I_n+\mu)^{-1},\\ \tilde{\mathbf{T}}_{21} &= -\sigma(I_n+\mu)\mathbf{D}^{-1}\mathcal{X}^{-1}\mathbb{1}_n\mathbb{1}_n^\top D + \mathbf{D}^{-1}\mathbf{B} - \kappa\mathcal{X}\mathcal{L}_C.\end{aligned}$$

Note that the scalar $\dot{\mathcal{V}}$ can be equivalently expressed as

$$\begin{aligned}\dot{\mathcal{V}} &= -\eta^\top\begin{bmatrix}\tilde{\mathbf{T}}_{11} & \tilde{\mathbf{T}}_{12}\\ \tilde{\mathbf{T}}_{21} & \tilde{\mathbf{T}}_{22}\end{bmatrix}\eta = -\frac{1}{2}\eta^\top\begin{bmatrix}\tilde{\mathbf{T}}_{11}+\tilde{\mathbf{T}}_{11}^\top & \tilde{\mathbf{T}}_{12}+\tilde{\mathbf{T}}_{21}^\top\\ * & \tilde{\mathbf{T}}_{22}+\tilde{\mathbf{T}}_{22}^\top\end{bmatrix}\eta\\ &:= -\eta^\top\begin{bmatrix}\mathbf{T}_{11} & \mathbf{T}_{12}\\ * & \mathbf{T}_{22}\end{bmatrix}\eta = -\eta^\top\mathbf{T}\eta,\end{aligned} \tag{4.13}$$

where

$$\begin{aligned}\mathbf{T}_{11} &= \frac{1}{2}\left(\tilde{\mathbf{T}}_{11}+\tilde{\mathbf{T}}_{11}^\top\right)\\ &= \varsigma(I_n+\mu)^{-1}D\\ &\quad - \tfrac{\sigma}{2}\left((I_n+\mu)M\mathbb{1}_n\mathbb{1}_n^\top\mathbf{D}^{-1}\mathbf{B}\mathcal{X}^{-1} + \mathbf{D}^{-1}\mathbf{B}\mathcal{X}^{-1}\mathbb{1}_n\mathbb{1}_n^\top M(I_n+\mu)\right),\\ \mathbf{T}_{22} &= \frac{1}{2}\left(\tilde{\mathbf{T}}_{22}+\tilde{\mathbf{T}}_{22}^\top\right)\\ &= \mathcal{X}\mathcal{L}_C\mathcal{X} + \tfrac{\sigma}{2}\left((I_n+\mu)\mathbf{D}^{-1}\mathcal{X}^{-1}\mathbb{1}_n\mathbb{1}_n^\top + \mathbb{1}_n\mathbb{1}_n^\top\mathbf{D}^{-1}\mathcal{X}^{-1}(I_n+\mu)\right),\\ \mathbf{T}_{12} &= \frac{1}{2}\left(\tilde{\mathbf{T}}_{12}+\tilde{\mathbf{T}}_{21}^\top\right)\\ &= \frac{1}{2}\left(-\varsigma(I_n+\mu)^{-1} - \sigma D\mathbb{1}_n\mathbb{1}_n^\top(I_n+\mu)\mathbf{D}^{-1}\mathcal{X}^{-1} + \mathbf{D}^{-1}\mathbf{B} - \kappa\mathcal{L}_C\mathcal{X}\right).\end{aligned}$$

Note that the entries of the matrix $\mathbf{T}$ in (4.13) are uncertain, because the clock drift matrix μ is uncertain. Hence, to obtain verifiable conditions that ensure $\mathbf{T} > 0$

and, thus, $\dot{\mathcal{V}}(\eta)$ being negative definite, we note that $\mathbf{T}$ can be decomposed as

$$\mathbf{T} = T - \frac{1}{2}\left(\Gamma_1\hat{T}_1 + \hat{T}_1^\top\Gamma_1\right) - \frac{1}{2}\left(\Gamma_2\hat{T}_2 + \hat{T}_2^\top\Gamma_2\right), \tag{4.14}$$

where T and $\hat{T}_2$ are defined in (4.4) and

$$\begin{aligned}\Gamma_1 &= \text{blkdiag}\left(\mu(I_n+\mu)^{-1}, \mu(I_n+\mu)^{-1}\right),\\ \Gamma_2 &= \text{blkdiag}\left(\mu,\mu\right), \quad \hat{T}_1 = \begin{bmatrix} \varsigma D & -\varsigma I_n \\ \mathbb{0}_{n\times n} & \mathbb{0}_{n\times n}\end{bmatrix}.\end{aligned} \tag{4.15}$$

For any matrices $A \in \mathbb{R}^{n\times n}$ and $B \in \mathbb{R}^{n\times n}$, it holds that (Horn and Johnson, 2012)

$$AB + B^\top A^\top \leq 2\|A\|_2\|B\|_2 I_n.$$

Therefore from (4.14), we have that

$$\mathbf{T} \geq T - \left(\|\hat{T}_1\|_2\|\Gamma_1\|_2 + \|\hat{T}_2\|_2\|\Gamma_2\|_2\right) I_{2n}. \tag{4.16}$$

Assumption 3.4 together with (4.3), implies that

$$\|\Gamma_1\|_2 \leq g_1(\epsilon), \quad \|\Gamma_2\|_2 \leq \epsilon,$$

where Γ_1 and Γ_2 are defined in (4.15). Therefore, (4.16) becomes

$$\mathbf{T} \geq T - \left(g_1(\epsilon)\|\hat{T}_1\|_2 + \epsilon\|\hat{T}_2\|_2\right) I_{2n}. \tag{4.17}$$

Furthermore, from (4.15), we have that

$$\|\hat{T}_1\|_2 = \sqrt{\lambda_{\max}(\hat{T}_1\hat{T}_1^\top)} = \varsigma\sqrt{\lambda_{\max}(D^2)+1}.$$

Turning to $\hat{T}_2$ defined in (4.4), we see that $\hat{T}_2$ depends on the control parameters $\mathbf{B}$ and $\mathbf{D}$. Therefore, to obtain $\|\hat{T}_2\|_2$ required in (4.17), we observe that

$$\begin{aligned} & \|\hat{T}_2\|_2 = \sqrt{\lambda_{\max}(\hat{T}_2\hat{T}_2^\top)} \leq \zeta\\ \Leftrightarrow \quad & \lambda_{\max}(\hat{T}_2\hat{T}_2^\top) \leq \zeta^2,\\ \Leftrightarrow \quad & \hat{T}_2\hat{T}_2^\top \leq \zeta^2 I_{2n},\\ \Leftrightarrow \quad & \frac{1}{\zeta}\hat{T}_2\hat{T}_2^\top - \zeta I_{2n} \leq 0,\end{aligned}$$

where $\zeta \in \mathbb{R}_{>0}$ is an upper bound for $\|\hat{T}_2\|_2$. By using the Schur complement (Horn and Johnson, 2012), the last inequality above is equivalent to the second inequality in (4.6). Thus, from (4.17) we see that $\mathbf{T} > 0$ if

$$T - \left(\varsigma g_1(\epsilon)\sqrt{\lambda_{\max}(D^2)+1} + \epsilon\zeta\right) I_{2n} > 0,$$

where ζ satisfies the second inequality in (4.6). Thus, with the made assumptions, $\mathbf{T} > 0$ implies that

$$\dot{\mathcal{V}}(\eta) < 0 \quad \text{for} \quad \eta(t) \neq \mathbb{0}_{2n}. \tag{4.18}$$

This shows that x^* is stable. Recall $\eta(t)$ defined in (4.12) and therefore, $\dot{\mathcal{V}}(\eta)$ does not depend on $\tilde{\theta}$.

Hence, to conclude local asymptotic stability of x^*, we need to show that the following implication holds along solutions of the system (4.2)

$$\mathbf{T}\eta(t) \equiv \mathbb{0}_{2n} \quad \Rightarrow \quad \lim_{t\to\infty} x(t) = x^*. \tag{4.19}$$

Since $\mathbf{T} > 0$ by assumption, the implication (4.19) is satisfied if and only if $\eta(t) = \mathbb{0}_{2n}$, which yields that $\tilde{\omega} = \mathbb{0}_n$ and $\tilde{p} = \mathbb{0}_n$. Furthermore, from (4.2), $\tilde{\omega} = \mathbb{0}_n$ implies that $\tilde{\theta}$ is constant. Moreover at $\eta(t) = \mathbb{0}_{2n}$, from the second equation in (4.2), we obtain that

$$\mathbb{0}_n = -\mathcal{R}\left[\nabla_{\tilde{\theta}}U(\delta(\tilde{\theta}+\theta^s)) - \nabla_{\tilde{\theta}}U(\delta(\theta^s))\right],$$

which by multiplying from the left with $\mathcal{R}^\top$ and rearranging terms is equivalent to

$$\mathcal{R}^\top\mathcal{R}\nabla_{\tilde{\theta}}U(\delta(\tilde{\theta}+\theta^s)) = \mathcal{R}^\top\mathcal{R}\nabla_{\tilde{\theta}}U(\delta(\theta^s)). \tag{4.20}$$

Note that $\mathcal{R}^\top\mathcal{R}$ is invertible and recall that $\nabla^2_{\tilde{\theta}}U(\delta(\tilde{\theta}+\theta^s))|_{\tilde{\theta}=\mathbb{0}_{n-1}} > 0$ (Schiffer et al., 2014, Lemma 5.8). Therefore, in a neighborhood of the origin, (4.20) only holds for $\tilde{\theta} = \mathbb{0}_{n-1}$. This shows that the implication (4.19) holds. Hence, x^* is locally asymptotically stable, completing the proof. □

Remark 4.2. *By fixing the tuning parameter σ, the design conditions* (4.5) *and* (4.6) *are a set of LMIs in ς, ζ, $\tilde{\mathbf{B}}, \mathbf{D}^{-1}$ and $\mathcal{L}_C$ that can be solved efficiently using standard software like Yalmip (Löfberg, 2004) within MATLAB®. Furthermore, the control parameters $\mathbf{B}$ and $\mathbf{D}$ can be easily recovered from $\tilde{\mathbf{B}} = \mathbf{D}^{-1}\mathbf{B}$ and $\mathbf{D}^{-1}$.*

5. Case study

In this section, the performance and robustness of the closed-loop MG model (3.1), (3.6) with DAI, pinning and GDAI control are compared via simulation. The MG (Figure 1) used in the case study is simulated using MATLAB®/Simulink® and PLECS (Plexim GmbH, 2013). In order to evaluate robustness towards further model uncertainties, lines are modeled with a small positive line resistance value. A constant impedance load of 500 kVA, unity power factor is connected at all GFIs. The time constant of the low pass filter used to measure the power output is 0.2 sec. To measure the synchronized electrical frequency ω^* (given in (3.12)) of the MG accurately, a conventional three-phase synchronous reference frame phase locked loop (SRF-PLL) (Golestan et al., 2012) is connected at the point of common coupling (PCC)[2].

[2]PCC is the point at which an islanded MG can be connected to the main grid (Lopes et al., 2006).

The weighting matrix $\mathcal{X}$ for the MG was fixed to (in pu)

$$\mathcal{X} = \text{diag}(0.02, 0.03, 0.03, 0.04, 0.05, 0.06, 0.06, 0.07), \tag{5.1}$$

and the vector of desired active power set point as (in pu)

$$P^d = \text{col}(0.25, 0.35, 0.45, 0.55, 0.65, 0.75, 0.80, 0.85). \tag{5.2}$$

The damping matrix D is chosen according to (2.15) with $\kappa = 0.2$. The incidence matrix $\mathcal{B}$ of the connected undirected graph mentioned in Section 2.1 is fixed in correspondence to the sparse communication topology shown in Figure 2. The reader is referred to (Fu et al., 2016; Alghamdi et al., 2018) for a comprehensive study on topology identification to implement similar distributed frequency control laws in power systems. In this section, we are interested in finding $\mathbf{D}$, $\mathbf{B}$ and the edge weight matrix $\mathbf{W}$ yielding $\mathcal{L}_C = \mathcal{B}\mathbf{W}\mathcal{B}^\top$ such that the LMIs (4.5) and (4.6) are feasible.

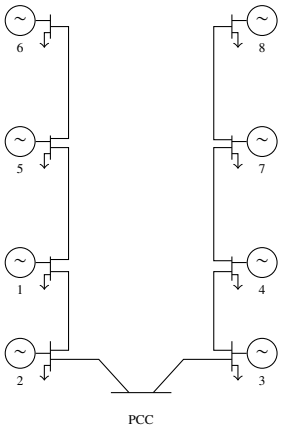

Figure 1: MG used in the simulation. There are eight GFIs, all of them having a constant impedance load connected to them. At the PCC, an SRF-PLL is connected to measure the synchronized electrical frequency ω^* (given by (3.12)) accurately. GFI1 is assumed to have the master clock, thus the clock drift matrix μ takes the form (5.3).

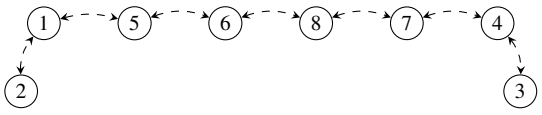

Figure 2: Topology of the communication network used in the simulation. This topology is used to calculate the incidence matrix $\mathcal{B} \in \mathbb{R}^{8\times7}$ required to build the Laplacian matrix $\mathcal{L}_C = \mathcal{B}\mathbf{W}\mathcal{B}^\top \in \mathbb{R}^{8\times8}$, where $\mathbf{W} \in \mathbb{R}^{7\times7}$ is the edge weight matrix.

The clock of GFI1 in Figure 1 is chosen as the master clock ($\mu_1 = 0$). The relative clock drift values of the other GFIs considered in the simulation (in sec) are

$$\mu = 10^{-4}\text{diag}(0, 3, 7, -3, 8, 5, -5, 2) \in \mathbb{R}^{8\times8}. \tag{5.3}$$

Hence, with the considered clock drift factors, $\epsilon = 0.001$ in Assumption 3.4.

The tuning criterion (4.5), (4.6) presented in Proposition 4.1 is verified with $\sigma = 10^{-6}$ using the optimization toolbox Yalmip (Löfberg, 2004) in MATLAB®/Simulink®. The feasibility of the conditions presented in (4.5), (4.6) ensures that the equilibrium point of the GDAI-controlled MG (4.1) is locally asymptotically stable in the presence of clock drifts. The control parameters satisfying (4.5), (4.6) were obtained as

$$\begin{aligned}
\mathbf{D} &= \text{diag}(132.5, 88.7, 90.8, 81.6, 84.6, 63.5, 69.0, 65.9),\\
\mathbf{B} &= \text{diag}(0.003, 0, 0, 0, 0, 0, 0, 0),\\
\mathbf{W} &= (0.01)\cdot\text{diag}(0.12, 0.06, 0.03, 0.03, 0.03, 0.03, 0.08).
\end{aligned} \tag{5.4}$$

Next, we simulate the MG shown in Figure 1 using the parameters (5.4). Note that in the simulation outputs, the term *power sharing ratios* denote $(P_i - P_i^{\text{net}})/\mathcal{X}_i, i \in \{1, \ldots, 8\}$, see also (2.14).

5.1. GDAI control

The GDAI-controlled system (4.1) is simulated using the control parameters (5.4). The simulation output is given in Figure 3 where until 10 sec, only the primary droop controller is in operation. The GDAI controller (3.25) is activated at 10 sec. Note that (3.25) satisfies the conditions in Lemma 3.6. Hence, we have $\omega^* = \omega^d$. See the enlarged frequency plot at 90 sec in Figure 3 where we can see that $\omega^* = 50$ Hz.

Furthermore, since (3.25) also satisfies the conditions of Lemma 3.8, steady-state power sharing is guaranteed in the presence of clock drifts. This can be confirmed by observing the enlarged power sharing ratio plot at 90 sec in Figure 3, where, it is clear that the power sharing ratios of all the GFIs converge to the same value. For better clarity, compare the enlarged power sharing ratio plots at 5 sec (droop control only: maximum relative deviation of approximately 42%) and 90 sec (droop with GDAI control: 0% relative deviation) in Figure 3. Hence correcting the steady-state deviations in power sharing ratios.

In order to compare the steady-state behavior of GDAI control with other distributed approaches, we implement the DAI control (3.8) and the pinning control (3.8) for the same MG given in Figure 1.

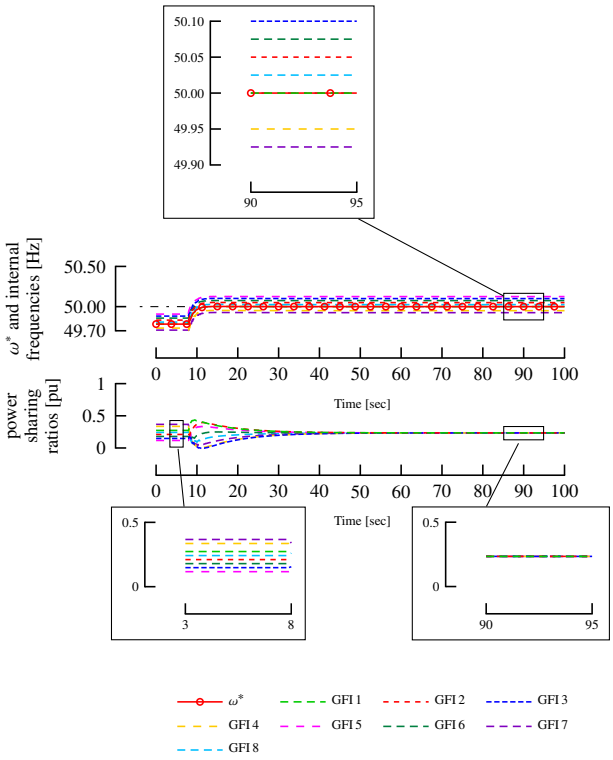

Figure 3: Simulation result with droop control (3.1) (active from 0 sec) and GDAI control (3.25) (activated at 10 sec). Note that ω^* converges exactly to 50 Hz and the power sharing ratios reach consensus, see the zoom plots at 90 sec.

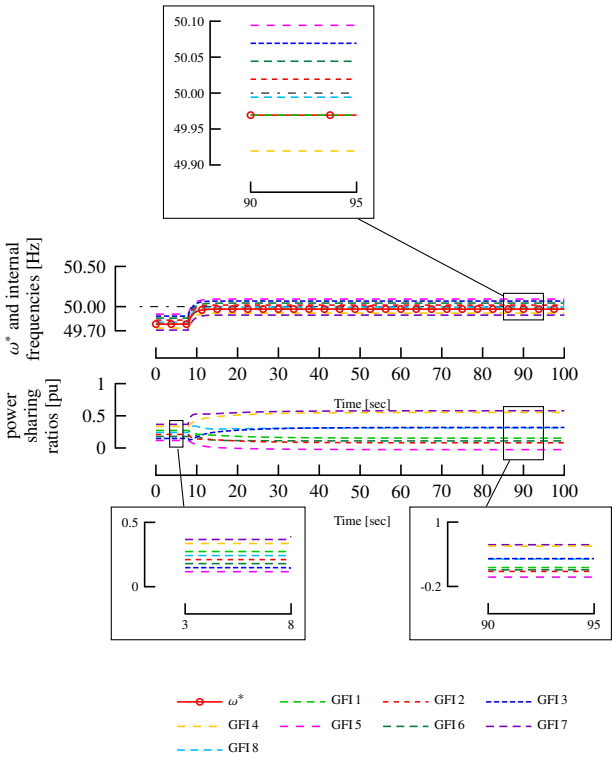

Figure 4: Simulation result with droop control (3.1) (active from 0 sec) and DAI control (3.6), (3.7) (activated at 10 sec). Note that ω^* does not converge to 50 Hz and the power sharing ratios do not reach consensus. See the zoom plots at 90 sec.

5.2. *DAI control*

We simulate the DAI-controlled system (3.1), (3.8) using the same parameters given in (5.4) with the only exception that $\mathbf{B}$ has all the diagonal entries equal to 0.003 yielding $\mathbf{B} > 0$. The simulation output is given in Figure 4, where until 10 sec, only the primary droop controller (3.1) (with $u = \mathbb{0}_8$) is in operation. The DAI controller (3.8) is activated at 10 sec. In Figure 4, we can see that the internal frequencies of the inverters converge close to the nominal value ($\omega^d = 50$ Hz), but not exactly to 50 Hz in the presence of clock drifts. Furthermore, the enlarged frequency plot in Figure 4 at 90 sec shows that $\omega^* \approx 49.97 \neq 50$ Hz. Hence resulting in a non-negligible steady-state network frequency error of approximately 30 mHz.

Considering the aspect of power sharing, when the DAI controller is activated on top of the droop controller at 10 sec, power sharing ratios diverge further. See the enlarged power sharing plots in Figure 4 at 5 sec (droop control only: maximum relative deviation of approximately 42%) and 90 sec (droop with DAI control: maximum relative deviation of approximately 60%) respectively. Hence, the performance in terms of power sharing in the presence of clock drifts is observed to be better with just the droop controller than a combination of droop and DAI controllers.

5.3. *Pinning control*

We simulate the pinning-controlled system (3.1), (3.10) using the MG shown in Figure 1 with the parameters given by (5.4). The simulation output is given in Figure 5, where until 10 sec, only the primary droop controller (3.1) (with $u = \mathbb{0}_8$) is under operation. The pinning controller (3.10) is activated at 10 sec. Note that the pinning gain matrix $\mathbf{B}$ is chosen such that $\mathbf{B}\mu = \mathbb{0}_{8\times 8}$. Hence, with ω^* defined in (3.12), we have $\omega^* = \omega^d$. See the enlarged frequency plot at 90 sec in Figure 5 where we can see that $\omega^* = 50$ Hz.

However, with regard to power sharing, the pinning controller is not able to correct deviations in power sharing ratios. Although in contrast to the DAI controller, power sharing ratios do not diverge as the pinning controller is activated. See the power sharing plot in Figure 5 at 5 sec (droop controller only) and 90 sec (droop

and pinning controller), where in both the cases, an approximate maximum relative deviation of 42% can be observed.

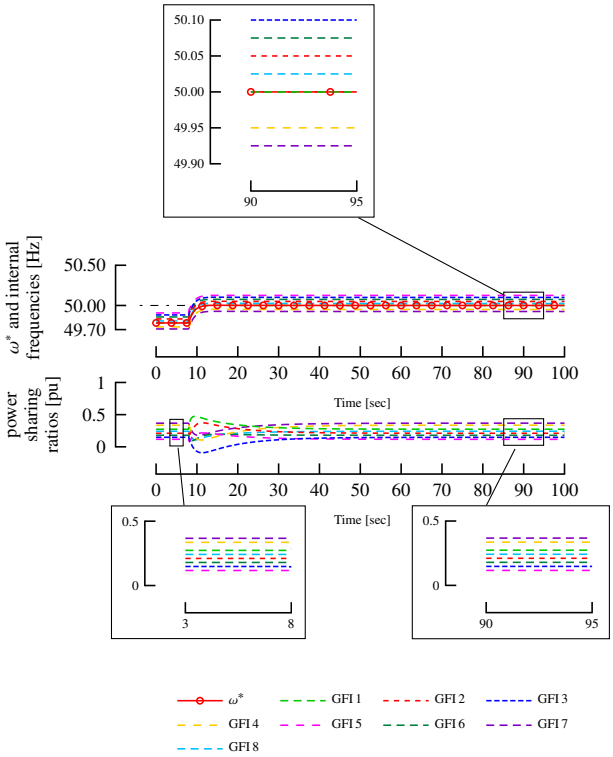

Figure 5: Simulation result with droop control (3.1) (active from 0 sec) and pinning control (3.6), (3.9) (activated at 10 sec). Note that ω^* converges exactly to 50 Hz. However, the power sharing ratios do not converge to a common value, i.e., no consensus. See the zoom plots at 90 sec.

Our observations are summarized in Table 1.

Objective/Control law	DAI	Pinning	GDAI
Accurate network frequency restoration	no	yes	yes
Accurate power sharing	no	no	yes

Table 1: Steady-state performance comparison of DAI, pinning and GDAI control in the presence of clock drifts.

6. Conclusions

In inverter-based MGs, clock drifts are a non-negligible phenomenon which can adversely affect the performance of secondary frequency control. In this paper, various distributed secondary frequency controllers are compared in the presence of clock drifts. Furthermore, necessary and sufficient conditions for steady-state accurate network frequency restoration and power sharing in the presence of clock drifts are derived. Based on these conditions, an alternative control law, called GDAI control, is proposed which achieves the aforementioned secondary control objectives. A tuning criterion which renders local asymptotic stability of the closed-loop equilibrium point with the GDAI controller in the presence of unknown bounded clock drifts is also presented. Finally, via simulation, the GDAI controller is compared with two other distributed frequency controllers in the literature.

Future research will incorporate time delays in communication network used in GDAI control. Also, we plan to test the GDAI controller on a real MG. Another interesting aspect is to consider time varying voltage amplitudes in the analysis.

Acknowledgment

J. Schiffer would like to thank K. Wulff for helpful comments and discussions on the proof of Proposition 4.1.

Appendix A. Remark on (3.10)

In the following we illustrate how (3.10) is the same as the control law presented in (Bidram et al., 2014). The primary frequency droop control (Bidram et al., 2014, Eq. 47) for the whole MG can be expressed in our notation as

$$\omega = -D^{-1}\left(\nabla U(\delta) - P^{\text{net}}\right) + u^{\text{sec}}, \qquad \text{(A.1)}$$

where $u^{\text{sec}} : \mathbb{R}_{\geq 0} \to \mathbb{R}^n$ is the secondary control input. Note that (A.1) represents the frequency dynamics in (3.1) with

- $\mu = \mathbb{0}_{n\times n}$ (yielding $\bar{\omega} = \omega$, see (2.5)),
- $\tau_P = \text{diag}(\tau_{P_i}) = \mathbb{0}_{n\times n} \Rightarrow M = \mathbb{0}_{n\times n}$,
- $\omega^d = 0$ and
- $u^{\text{sec}} = D^{-1}u$.

Furthermore, the secondary frequency control law proposed in (Bidram et al., 2014, Eq. 52,53) for the whole network can be expressed in our notation as

$$u = p,$$
$$\dot{p} = -C_F\left[(\mathcal{B} + \mathcal{L}_C)(\omega - \mathbb{1}_n\omega^d) + \mathcal{L}_C D^{-1}\left(\nabla U(\delta) - P^{\text{net}}\right)\right],$$

where $C_F > 0$ and $\mathcal{B} \geq 0$ are diagonal controller matrices and $\mathcal{L}_C \in \mathbb{R}^{n\times n}$ is the Laplacian matrix of the communication graph. Inserting $D^{-1}\left(\nabla U(\delta) - P^{\text{net}}\right)$ from (A.1) in the above control law yields

$$\begin{aligned}\dot{p} &= -C_F\mathcal{B}(\omega - \mathbb{1}_n\omega^d) - C_F\mathcal{L}_C u^{\text{sec}},\\ &= -C_F\mathcal{B}(\omega - \mathbb{1}_n\omega^d) - C_F\mathcal{L}_C D^{-1}p,\\ &= -C_F\mathcal{B}(\omega - \mathbb{1}_n\omega^d) - \frac{1}{\kappa}C_F\mathcal{L}_C\mathcal{X}p,\end{aligned}$$

where we have used $u^{\text{sec}} = D^{-1}u = D^{-1}p$ and (2.15). For $C_F = \kappa\mathbf{D}\mathcal{X}$ and $C_F\mathcal{B} = \mathbf{B}$, the control law described above is the same as (3.10).

References

Alghamdi, S., Schiffer, J., Fridman, E., 2018. Distributed secondary frequency control design for microgrids: Trading off l2-gain performance and communication efforts under time-varying delays. In: European Control Conference. pp. 758 – 763.

Anderson, P., Fouad, A., 2002. Power System Control and Stability. J.Wiley & Sons.

Anritsu, 2001. Understanding frequency accuracy in crystal controlled instruments - application note. Tech. rep., Anritsu EMEA Ltd.

Bidram, A., Davoudi, A., 2012. Hierarchical structure of microgrids control system. IEEE Transactions on Smart Grid 3 (4), 1963–1976.

Bidram, A., Lewis, F., Davoudi, A., 2014. Distributed control systems for small-scale power networks: Using multiagent cooperative control theory. IEEE Control Systems Magazine 34 (6), 56–77.

Castilla, M., Camacho, A., Martí, P., Velasco, M., Ghahderijani, M. M., 2017. Impact of clock drifts on communication-free secondary control schemes for inverter-based islanded microgrids. IEEE Transactions on Industrial Electronics, 4739 – 4749.

Castilla, M., Camacho, A., Miret, J., Velasco, M., Marti, P., 2018. Local secondary control for inverter-based islanded microgrids with accurate active-power sharing under high load conditions.

Chandorkar, M., Divan, D., Adapa, R., Jan/Feb 1993. Control of parallel connected inverters in standalone AC supply systems 29 (1), 136 –143.

Diestel, R., 2010. Graph Theory, 4th Edition. Springer.

Dörfler, F., Simpson-Porco, J. W., Bullo, F., Sept. 2016. Breaking the hierarchy: Distributed control & economic optimality in microgrids. IEEE Transactions on Control of Network Systems 3 (3), 241 – 253.

Farhangi, H., Jan/Feb 2010. The path of the smart grid. IEEE Power and Energy Magazine 8 (1), 18 –28.

Fu, X., Dörfler, F., Jovanović, M. R., 2016. Topology identification and design of distributed integral action in power networks. In: American Control Conference (ACC). pp. 5921 – 5926.

Godsil, C., Royle, G., 2001. Algebraic Graph Theory. Springer.

Golestan, S., Monfared, M., Freijedo, F. D., Feb. 2012. Design-oriented study of advanced synchronous reference frame phase-locked loops 28, 765–778.

Guerrero, J., Loh, P., Chandorkar, M., Lee, T., 2013. Advanced control architectures for intelligent microgrids – part I: Decentralized and hierarchical control. IEEE Transactions on Industrial Electronics 60 (4), 1254–1262.

Hans, C. A., Nenchev, V., Raisch, J., Reincke-Collon, C., 2014. Minimax model predictive operation control of microgrids, 19th IFAC World Congress, Cape Town, South Africa.

Hatziargyriou, N., Asano, H., Iravani, R., Marnay, C., 2007. Microgrids. IEEE Power and Energy Magazine 5 (4), 78–94.

Horn, R. A., Johnson, C. R., 2012. Matrix analysis. Cambridge university press.

Kolluri, R. R., Mareels, I., Alpcan, T., Brazil, M., de Hoog, J., Thomas, D. A., 2017. Power sharing in angle droop controlled microgrids. IEEE Transactions on Power Systems 32 (6), 4743 – 4751.

Kolluri, R. R., Mareels, I., Alpcan, T., Brazil, M., de Hoog, J., Thomas, D. A., 2018. Stability and active power sharing in droop controlled inverter interfaced microgrids: Effect of clock mismatches. Automatica 93, 469–475.

Kopetz, H., 2011. Real-time systems: design principles for distributed embedded applications. Springer.

Krishna, A., Hans, C. A., Schiffer, J., Raisch, J., Kral, T., 2017. Steady state evaluation of distributed secondary frequency control strategies for microgrids in the presence of clock drifts. In: 25th Mediterranean Conference on Control and Automation (MED). pp. 508 – 515.

Krishna, A., Schiffer, J., Raisch, J., 2018. A consensus-based control law for accurate frequency restoration and power sharing in microgrids in the presence of clock drifts. In: European Control Conference (ECC). pp. 2575 – 2580.

Kundur, P., 1994. Power system stability and control. McGraw-Hill.

Lasseter, R., 2002. Microgrids. In: IEEE Power Engineering Society Winter Meeting, 2002. Vol. 1. pp. 305 – 308 vol.1.

Löfberg, J., Sept. 2004. YALMIP : A toolbox for modeling and optimization in MATLAB. In: IEEE International Symposium on Computer Aided Control Systems Design. pp. 284 –289.

Lopes, J., Moreira, C., Madureira, A., May 2006. Defining control strategies for microgrids islanded operation. IEEE Transactions on Power Systems 21 (2), 916 – 924.

Machowski, J., Bialek, J., Bumby, J., 2008. Power system dynamics: stability and control. J.Wiley & Sons.

Majumder, R., Ledwich, G., Ghosh, A., Chakrabarti, S., Zare, F., Oct. 2010. Droop control of converter-interfaced microsources in rural distributed generation. IEEE Transactions on Power Delivery 25 (4), 2768–2778.

Martí, P., Torres-Martínez, J., Rosero, C. X., Velasco, M., Miret, J., Castilla, M., Dec. 2018. Analysis of the effect of clock drifts on frequency regulation and power sharing in inverter-based islanded microgrids. IEEE Transactions on Power Electronics 33 (12), 10363 – 10379.

Martínez, J. T., Castilla, M., Miret, J., Ghahderijani, M. M., Rey, J. M., 2017. Experimental study of clock drift impact over droop-free distributed control for industrial microgrids. In: 43rd Annual Conference of the IEEE Industrial Electronics Society , IECON. pp. 2479 – 2484.

Mesbahi, M., Egerstedt, M., 2010. Graph theoretic methods in multiagent networks. Princeton University Press.

Olfati-Saber, R., Fax, J. A., Murray, R. M., 2007. Consensus and cooperation in networked multi-agent systems. Proceedings of the IEEE 95 (1), 215–233.

Pai, M. A., 1989. Energy function analysis for power system stability. Kluwer academic publishers.

Persis, C. D., Monshizadeh, N., Jan. 2017. Bregman storage functions for microgrid control. IEEE Transactions on Automatic Control 63 (1), 53 – 68.

Persis, C. D., Monshizadeh, N., Schiffer, J., Dörfler, F., 2016. A Lyapunov approach to control of microgrids with a network-preserved differential-algebraic model. In: CDC. pp. 2595 – 2600.

Plexim GmbH, 2013. Plecs software, www.plexim.com.

Rosero, C. X., Carrasco, H., Velasco, M., Martí, P., 2017a. Impact of clock drifts on active power sharing and frequency regulation in distributed-averaging secondary control for islanded microgrids. In: International Autumn Meeting on Power, Electronics and Computing. pp. 1 – 6.

Rosero, C. X., Martí, P., Velasco, M., Castilla, M., Miret, J., Camacho, A., 2017b. Consensus for active power sharing and frequency restoration in islanded microgrids subject to drifting clocks. In: IEEE 26th International Symposium on Industrial Electronics (ISIE). pp. 70 – 75.

Schenato, L., Fiorentin, F., 2011. Average timesynch: A consensus-based protocol for clock synchronization in wireless sensor networks. Automatica 47 (9), 1878–1886.

Schiffer, J., 2015. Stability and power sharing in microgrids. Ph.D. thesis, Technische Universität Berlin.

Schiffer, J., Dörfler, F., 2016. On stability of a distributed averaging PI frequency and active power controlled differential-algebraic power system model. In: European Control Conference (ECC). pp. 1487 – 1492.

Schiffer, J., Dörfler, F., Fridman, E., 2017a. Robustness of distributed averaging control in power systems: Time delays & dynamic communication topology. Automatica 80, 261–271.

Schiffer, J., Hans, C. A., Kral, T., Ortega, R., Raisch, J., 2017b. Modeling, analysis, and experimental validation of clock drift effects in low-inertia power systems 64, 5942 – 5951.

Schiffer, J., Ortega, R., Astolfi, A., Raisch, J., Sezi, T., 2014. Conditions for stability of droop-controlled inverter-based microgrids. Automatica 50 (10), 2457–2469.

Schiffer, J., Ortega, R., Hans, C., Raisch, J., 2015. Droop-controlled inverter-based microgrids are robust to clock drifts. American Control Conference, 2341 – 2346.

Simpson-Porco, J. W., Dörfler, F., Bullo, F., 2013. Synchronization and power sharing for droop-controlled inverters in islanded microgrids. Automatica 49 (9), 2603 – 2611.

Simpson-Porco, J. W., Shafiee, Q., Dörfler, F., Vasquez, J. C., Guerrero, J. M., Bullo, F., 2015. Secondary frequency and voltage control of islanded microgrids via distributed averaging. IEEE Transactions on Industrial Electronics 62, 7025–7038.

Solis, R., Borkar, V. S., Kumar, P. R., 2006. A new distributed time synchronization protocol for multihop wireless networks. In: CDC. pp. 2734 – 2739.

van der Schaft, A., 2000. L2-Gain and Passivity Techniques in Nonlinear Control. Springer.

Weitenberg, E., Jiang, Y., Zhao, C., Mallada, E., Persis, C. D., Dörfler, F., 2018. Robust decentralized secondary frequency control in power systems: Merits and trade-offs. IEEE Transactions on Automatic Control (Early Access).

Zhao, C., Mallada, E., Dörfler, F., July 2015. Distributed frequency control for stability and economic dispatch in power networks. In: American Control Conference (ACC). pp. 2359 – 2364.